Determining the Importance of Initiation Mechanism and Background Environment on the Evolution of Deep Convection in Varied Regimes

Christopher J. Nowotarski, Anita D. Rapp, Milind Sharma, Sarah D. Brooks, Bo Chen | *Texas A&M University Department of Atmospheric Sciences*

Motivation

Results from the TRACER field campaign suggest that despite differences in both thermodynamic and aerosol environments between observed convective cells on opposite sides of the sea-breeze front, the strongest cells were those initiated by and remaining near the sea-breeze front.[1,2]

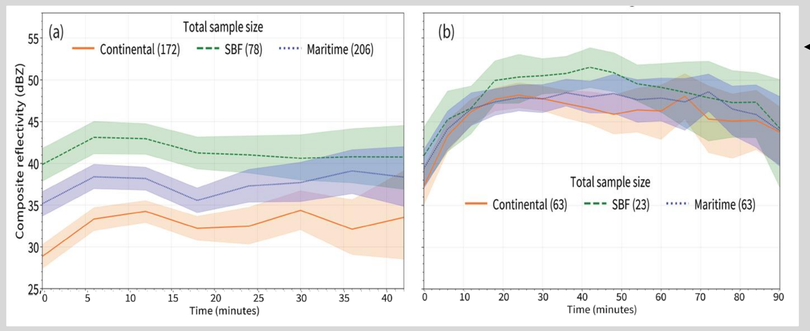

Time series of (a) shallow and (b) deepening cell composite reflectivity as a function of sea-breeze front (SBF) relative location[2]

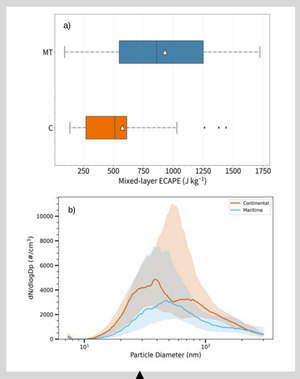

Distributions of (a) entrainment CAPE (ECAPE) and aerosol size distributions for cell environments on the maritime (MT) and continental (CT) sides of the SBF[2,3]

Given the apparent sensitivity of convection's intensity to its initiation mechanism and meso/synoptic scale dynamic forcing, our current project investigates the overarching question: **In what regimes is convection more sensitive to its initiation mechanism compared to the background meteorological or aerosol environment?**

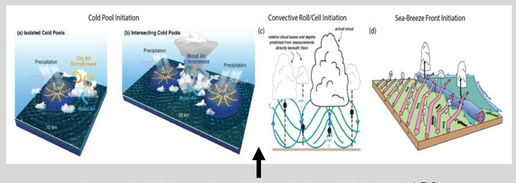

Potential CI mechanisms during TRACER[4,5,6]

KEY SCIENCE QUESTIONS

What fraction of shallow and deep convective cells were associated with various initiation mechanisms during the TRACER campaign?

What initiation mechanism typically provides the widest, strongest nascent updrafts?

Is the nascent cell updraft width or strength more important to subsequent evolution than background aerosol or meteorological environment?

Do bulk statistics of convection from coarse simulations that rely on convective parameterizations differ from high-resolution simulations with better resolved initiation and cloud-scale processes?

How do different regimes, including those at the new SEUS ARM site, affect the answers to these questions?

Methods

We are building a dataset of isolated convective cells from TRACER and the new SEUS ARM campaigns, matched to their initiation mechanism, with observed cell and environment attributes, including "nascent" shallow cumulus cloud top vertical velocity and width (as a proxy for CI characteristics) and background large-scale ascent. Case-studies of specific initiation mechanisms will be modeled using WRF to understand storm-scale dynamics and microphysics.

Table of variables matched to each cell with observation platforms and availability during TRACER

Atmospheric Variable Matched to Cell	Instrument/Source	TRACER Sites/Group
Nascent Cell Cloud Top Vertical Velocity Retrieval	GOES East IR	Full coverage
Nascent Cell Width	NEXRAD, GOES East VIS	Full coverage
Background near-cell thermodynamic environment profiles and derived parameters (e.g., CAPE, CIN, tropospheric RH)	Radiosondes, AMDAR soundings, surface meteorological observations, interpolatedsonde	AMF1, ANC, TAMU TRACER, IAH, HOU
Background near-cell kinematic environment profiles and derived parameters (e.g., vertical wind shear, storm-relative flow)	Radiosondes, AMDAR soundings, Doppler lidar, radar wind profiler, surface meteorological observations, interpolatedsonde	AMF1, ANC, TAMU TRACER, IAH, HOU
Background large-scale ascent in lower and mid troposphere	ERA5 Reanalysis	Full coverage
Background near-cell surface and lower tropospheric profiles of CCN and INP concentration	CCN counters, condensation particle counters, DRUM aerosol samplers (for offline INP analysis), micropulse lidar	AMF1, ANC, TAMU TRACER

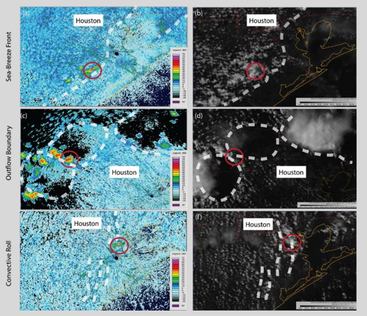

Example of isolated cells initiated by (top) sea-breeze front, (middle) outflow boundaries, and (bottom) convective rolls during TRACER. Each cell in the dataset needs to be categorized by CI mechanism.

Nascent cell identified on radar and visible satellite. Cloud-top vertical velocity will be estimated as $w \approx \gamma_m^{-1} \frac{\Delta T_B}{\Delta t}$ *where* γ_m *is the moist adiabatic lapse rate and* ΔT_B *is the change in infrared satellite brightness temperature.*[7]

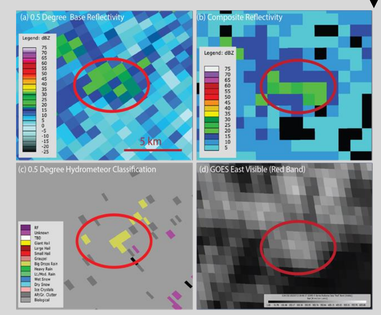

Progress and Challenges with Nascent Cell Tracking

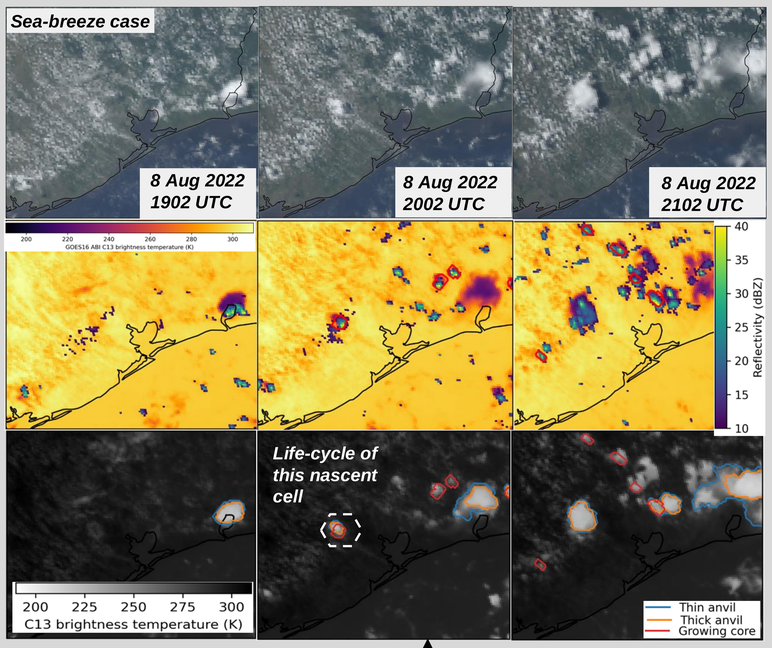

Example cell tracking with (top) GOES 16 true color, (middle) KHGX radar reflectivity and GOES 16 T_{B13}*, and (bottom)* T_{B13} *matched to tracked cells.*

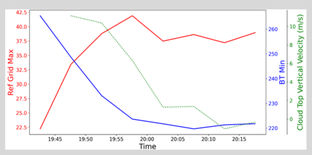

Maximum reflectivity (red), minimum clean IR brightness temperature (blue), and derived cloud-top vertical velocity (green) for a tracked nascent cell.

(i) We use tobac-flow[8] to track convective cores detected from GOES16 ABI water vapor difference (WVD; T_{B8}-T_{B10}) field such that WVD ≥ 0.5 K min^{-1} for at least 15 minutes. Anvils (thin and thick) are detected using WVD and split window difference (SWD; T_{B13}-T_{B15}) fields.

(ii) Particle Image Velocimetry[9]: Tracks cloud objects using only ABI L2 cloud mask product (ACM). Performance issues in the presence of cirrus clouds (large cloud mask).

(iii) Flexible cloud tracking using multivariate data (e.g., combined radar and satellite observations) in tobac[10] or PyFLEXTRKR[11]. Radar-based cloud tracking may miss the nascent cells.

***Challenges:* Fine-tune the detection of nascent convective cores earlier in shallow stage when cloud tops are still largely forced by CI mechanism.**

Observed Aerosol Profile Curve Fitting

With surface aerosol size distributions and micropulse lidar (MPL) data, we have built vertical profiles of observed aerosol profiles and their CCN/INP capability in convective environments during TRACER.[12] However, not all sites have full information (e.g., TRACER ANC site), so we are developing a curve-fitting procedure to replicate vertical profiles without an MPL.

Curve fitting function for parameterizing aerosol vertical profile:

$$X(r) = \frac{X_0 - X_f}{1+f} \cdot \frac{1 + fe^{-\frac{r}{\gamma}}}{1 + \left(\frac{r}{r_m}\right)^{r_m k}} + X_f$$

Demonstration of effect of each term on fitted profile shape

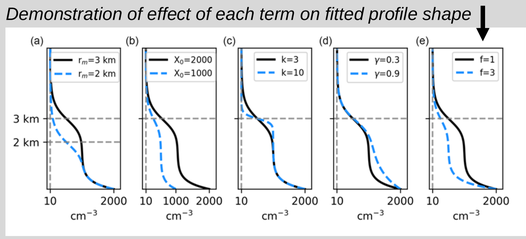

Example fit (green) to observed profile (black) based on MPL backscatter (lower right curtain plot) on 18 May 2022

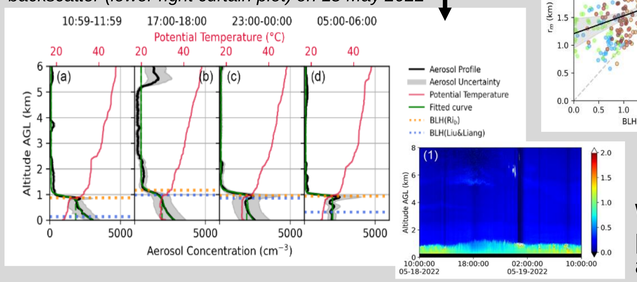

Demonstration of predicting aerosol vertical profile using fitting function

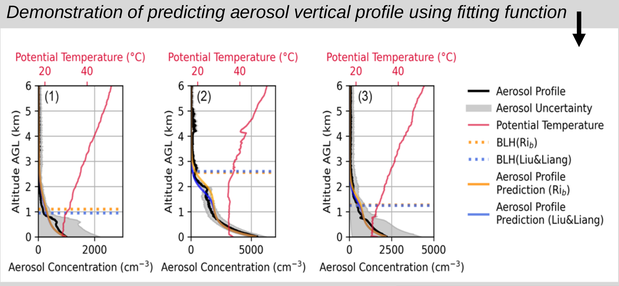

Comparison between fitted rm and PBL height

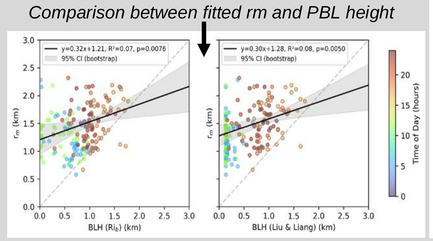

Comparison between fitted k and potential temperature gradient at rm

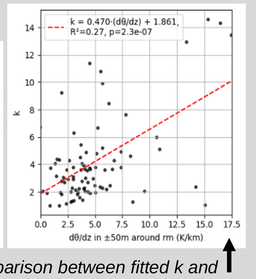

While there is a correlation, the thermodynamic profile alone may be insufficient to explain aerosol vertical distributions. Work continues…

This research is funded by DOE ASR grant DE-SC0025215.

1. Rapp, A. D., S. D. Brooks, C. J. Nowotarski, M. Sharma, S. A. Thompson, B. Chen, B. Matthews, M. Etten-Bohm, E. R. Nielsen, and R. Li, 2024: TAMU TRACER: Targeted mobile measurements to isolate the impacts of aerosols and meteorology on deep convection. Bull. Amer. Meteor. Soc., E1685-E1702.
2. Sharma, M., A. D. Rapp, C. J. Nowotarski, and S. D. Brooks, 2024: Observed variability in convective cell characteristics and near-storm environments across the sea and bay-breeze fronts in southeast Texas. Mon. Wea. Rev., 152, 2419-2441.
3. Thompson, S. A., B. Chen, B. H. Matthews, R. Li, C. J. Nowotarski, A. D. Rapp, and S. D. Brooks, 2025: Characterizing greater Houston's aerosol by airmass during TRACER. J. Geophys. Res.: Atmospheres, in review.
4. Feng, Z., S. Hagos, A. K. Rowe, C. D. Burleyson, M. N. Martini, and S. P. de Szoeke, 2015: Mechanisms of convective cloud organization by cold pools over tropical warm ocean during the AMIE/DYNAMO field campaign. J. Advances in Modeling Earth Systems, 7, 357-381.
5. Weckwerth, T. M., J. W. Wilson, and R. M. Wakimoto, 1996: Thermodynamic variability within convective boundary layer due to horizontal convective rolls. Mon. Wea. Rev., 124, 769-784.
6. Atkins, N. T., R. M. Wakimoto, and T. M. Weckwerth, 1995: Observations of the sea-breeze front during CaPE. Part II: Dual-Doppler and aircraft analysis. Mon. Wea. Rev., 123, 944-969.
7. Hamada, A., and Y. N. Takayabu, 2016: Convective cloud top vertical velocity estimated from geostationary satellite rapid-scan measurements. Geophys. Res. Lett., 43, 5435-5441.
8. Jones, W.K., Stengel, M. and Stier, P., 2024: A Lagrangian perspective on the lifecycle and cloud radiative effect of deep convective clouds over Africa. Atmospheric Chemistry and Physics, 24(9), 5165-5180.
9. Seelig, T., Deneke, H., Quaas, J. and Tesche, M., 2021: Life cycle of shallow marine cumulus clouds from geostationary satellite observations. Journal of Geophysical Research: Atmospheres, 126(22), p.e2021JD035577.
10. Sokolowsky, G.A., Freeman, S.W., Jones, W.K., Kukulies, J., Senf, F., Marinescu, P.J., Heikenfeld, M., Brunner, K.N., Bruning, E.C., Collis, S.M. and Jackson, R.C., 2024: tobac v1. 5: introducing fast 3D tracking, splits and mergers, and other enhancements for identifying and analysing meteorological phenomena. Geoscientific Model Development, 17(13), 5309-5330.
11. Feng, Z., Hardin, J., Barnes, H.C., Li, J., Leung, L.R., Varble, A. and Zhang, Z., 2023. PyFLEXTRKR: A flexible feature tracking Python software for convective cloud analysis. Geoscientific Model Development, 16(10), 2753-2776.
12. Chen, B., S. A. Thompson, B. H. Matthews, M. Sharma, R. Li, C. J. Nowotarski, A. D. Rapp, and S. D. Brooks, 2025: A new technique to retrieve aerosol vertical profiles using the micropulse lidar and ground-based aerosol measurements. Atmos. Meas. Tech., in review.